Enhanced HDN Performance of Al, Zr and Ti Modified NiW Catalysts by Using Co-Impregnation Method

Fang Guo*[+], ***Yi-en Du, Xianjun Niu***
College of Chemistry and Chemical Engineering, Jinzhong University, Jinzhong 030600, P.R. CHINA

Shaoqing Guo, Xianxian Wei
College of Environment and Safety, Taiyuan University of Science and Technology, Taiyuan 030024, P.R. CHINA

Xiaoxiao Wang
School of Chemical and Biological Engineering, Taiyuan University of Science and Technology, Taiyuan 030001, P.R. CHINA

Zegang Qiu
College of chemistry and chemical engineering, Xi'an University of Petroleum, Xi'an 710065, P.R. CHINA

Liangfu Zhao
Laboratory of Applied Catalysis and Green Chemical Engineering, Institute of Coal Chemistry, Chinese Academy of Sciences, Taiyuan 030001, P.R. CHINA

ABSTRACT: *The Al, Zr, and Ti modified MCM-41 materials were prepared by post-synthesis method, and then the Ni-W species were introduced on them by using the co-impregnation method to obtain high-performance hydrodenitrogenation (HDN) catalysts. The activity of the catalysts was evaluated by the HDN reaction of quinoline. The optimum HDN activity was observed on the catalyst supported on the Al modified MCM-41. The high performance of the NiW/Al catalyst was due to the higher dispersion of Ni, W species, the more density of acid sites, the more appropriate nature of W species, and the lower reduction temperature of W species. Moreover, the catalysts prepared by co-impregnation method showed better performance than the catalysts prepared by the sequential impregnation method in the HDN of quinoline.*

KEYWORDS: *Al, Zr, Ti modified MCM-41; NiW catalyst; Co-impregnation; Hydrodenitrogenation;*

***** *To whom correspondence should be addressed.*
+ E-mail: guofang110119@163.com
1021-9986/2019/6/69-81 13/$/6.03

INTRODUCTION

The nitrogen compounds in the heavy oils could generate serious environmental pollution. Hydrodenitrogenation (HDN) can remove nitrogen from petroleum feedstocks, which providing more processable and environmentally transportation fuels. In practice, HDN is carried out simultaneously with hydrodesulfurization (HDS) in the presence of catalysts, yet HDN is less well-studied than HDS [1]. Meanwhile, the nitrogen compounds in the heavy oils can accelerate the deactivation of catalyst. Therefore, it is necessary to remove the nitrogen compounds in the heavy oils and pay more attention to the investigation of the HDN.

Generally, the Al_2O_3 as a conventional support for HDS and HDN has desirable properties, such as high mechanical strength and low cost. However, it provides too strong metal-support interaction [2]. The TiO_2 and ZrO_2 have attracted attention due to the higher intrinsic HDS activity. However, the TiO_2 and ZrO_2 have low surface areas [3, 4]. Recently, well-ordered mesoporous silica such as MCM-41 has attracted considerable interest due to its high surface areas and homogeneous pore diameters. However, the MCM-41 provides very low metal-support interaction [5]. Therefore, the researchers try to combine the Al_2O_3, TiO_2 and ZrO_2 with the MCM-41 to take advantage of the overall properties of them [6-9]. It was reported that the MCM-41 modified by Al, Zr and Ti have been used as supports for HDS catalysts and offer certain advantage in the HDS [6-8]. In our previous work [9], the NiW catalysts prepared by sequential impregnation method using Al, Zr and Ti modified MCM-41 as supports showed significant improvement in the HDN activity of quinoline.

As everyone knows, the impregnation method of catalysts plays an important role in the precursor structure of catalysts and in the activity of catalysts. It was reported that the impregnation method significantly affected the structure, dispersion and chemical states of metal species on the catalysts [10, 11]. As mentioned above, the sequential impregnation method was used to prepare the NiW catalysts using Al, Zr and Ti modified MCM-41 as supports, which showed significant improvement in the HDN activity of quinoline [9]. Therefore, in the present study, the co-impregnation method was taken to prepare the NiW catalysts using Al, Zr and Ti modified MCM-41 as supports. The aim is to study the effects of the incorporation of Al, Zr and Ti into MCM-41 on the structure and performance for HDN of quinoline over the NiW catalysts prepared by co-impregnation method. Moreover, the difference in properties of catalysts which prepared by different impregnation methods were also discussed.

EXPERIMENTAL SECTION

Preparation of Catalysts

The MCM-41 was supplied by the Catalyst Plant of Nankai. The modified supports were prepared by postsynthetic method described in our previous work [9]. They were prepared in the following way. Aluminium isopropoxide ($Al(i\text{-}PrO)_3$, 99 %, Aldrich), zirconium propoxide ($Zr(n\text{-}PrO)_4$, 70 wt.% solution in 1-propanol, Aldrich), Titanium isopropoxide ($Ti(i\text{-}PrO)_4$, 97 %, Aldrich) were used as Al, Zr and Ti sources, respectively. Isopropanol was used as solvent. In the postsynthetic procedure, calcined MCM-41 materials were impregnated in isopropanol containing $Al(i\text{-}PrO)_3$, $Zr(n\text{-}PrO)_4$ or $Ti(i\text{-}PrO)_4$ for 12 h at room temperature. The samples were then dried at 80 ^oC for 12 h and calcined at 550 ^oC for 6 h. The modified supports were denoted as Al-MCM-41, Zr-MCM-41 and Ti-MCM-41, respectively. The nominal atomic ratio of M/Si (M=Al, Zr or Ti) is 0.025 for all the modified supports.

The W precursor and Ni precursor of the catalysts were the ammonium paratungstate and nickel nitrate hexahydrate (analytical grade), respectively. The catalysts were prepared by co-impregnation method using an equilibrium-adsorption technique. In this method, the MCM-41 was impregnated with a solution containing a mixture of W and Ni precursors salts. After impregnation, the samples were dried at room temperature for 12 h and then at 80 ^oC for 12 h. Finally, the calcination was performed at 540 ^oC for 3 h. All the catalysts were prepared with the same amounts of WO_3 and NiO, their nominal amounts were 20 wt.% and 2.5 wt.%, respectively. The prepared catalysts were designated as NiW or NiW/X (X=Al, Zr and Ti). Moreover, as a representation of catalysts prepared by sequential impregnation method, the Ni/W/Al catalyst was prepared by sequential impregnation method using Al modified MCM-41 as support.

Characterization Techniques

The X-ray diffraction (XRD) were recorded on a Bruker D8 Advance diffractometer with Cu Kα radiation

(λ=1.54178 Å). The power diffractograms were recorded in the 2θ range of 0.5-80 ° at a step of 0.01 ° s^{-1}.

N_2 adsorption-desorption isotherms were recorded on a Tristar-3000 Micromeritics volumetric apparatus. The special surface area was calculated according to the BET isothermal equation. The pore diameter was calculated by applying the Barret-Joyner-Halenda (BJH) method to the adsorption branches of the N_2 isotherms. The pore volume was obtained for the isotherms at P/P_o = 0.99.

Laser Raman spectra were recorded on a LabRAM HR800 System with a CCD detector at room temperature. The 325 nm of the He-Cd laser was employed as the exciting source with a power of 30 MW.

The XPS spectra were measured by using a Kratos XSAM800 fitted with an Al Kα source (1486.6 eV) with two ultra-high-vacuum (UHV) chambers. The binding energy was referenced to the C1s peak (284.8 eV) to account for charging effects. The areas of the peaks were computed after fitting of the experimental spectra to Gaussian/Lorentzian curves and removal of the background (Shirley function). Surface atomic ratios were calculated from the peak area ratios normalized by the corresponding atomic sensitivity factors.

IR spectra of adsorbed pyridine (Py-IR) were recorded using a Nicolet-510P apparatus. Prior to the pyridine adsorption, the calcined samples were pressed into thin wafers and evacuated in situ under vacuum at 300 °C for 2 h, then cooled to room temperature, and successive pyridine was dosed until saturated adsorption on the samples. Finally, the system was evacuated at different temperatures and pyridine-adsorbed IR spectra were recorded.

TPR experiments were carried out in a AutoChem II 2920 equipment (Micromeritics, USA) using 0.01 g catalysts for each run. Typically, the catalysts were pretreated in Ar at 550 °C for 2h and then cooled at 30 °C. Subsequently, the Ar flow was switched to 10 % H_2-Ar mixed gas. The H_2-TPR was started from 30 °C to 900 °C at a heating rate of 10 °C/min and simultaneously monitored by a Thermal Conductivity Detector (TCD).

Scanning Electron Microscopy (SEM) was performed using a JSM-7001F.

Catalytic Activity Test

The HDN reaction of quinoline was carried out in a fixed-bed reactor (a 50 cm long stainless steel tube with an inner diameter of 6 mm) with the feed of quinoline in n-heptane (0.5 wt.% N). The reactor was charged with 1 g catalyst in 20-40 mesh size. Prior to the reaction, the catalyst was in-situ presulfided at 400 °C and 3 MPa for 3 h with a 3 mL/h feed of 5 % CS_2 in n-hexane. After that, the HDN reaction was carried out under the conditions (pressure of 4 MPa, temperature of 350-390 °C at a step of 20 °C, WHSV of 2 h^{-1} and H_2/feed volumetric ratio of 1000). Then after a stabilization period of 12 h, the reaction products were condensed and periodically separated from a gas-liquid separator. The reaction products were analyzed by a 5860 gas chromatograph equipped with a flame ionization detector and a capillary column (DB-5).

RESULTS AND DISCUSSION

XRD of supports and catalysts

The small-angle XRD patterns and wide-angle XRD patterns of supports are shown in Fig. 1A and B, respectively. As described in our previous work [9], the modified supports of Al-MCM-41, Zr-MCM-41 and Ti-MCM-41 can be prepared without lose of the MCM-41 mesoporous structure and with highly dispersed Al, Zr and Ti species.

The wide-angle XRD patterns of catalysts are shown in Fig. 2. It can be found that the wide-angle XRD patterns of catalysts are similar with that of the supports. No crystalline phases are detected, suggesting that the Ni and W species are well dispersed for all the catalysts [13].

N_2 adsorption-desorption of supports and catalysts

The textural properties of the supports and catalysts are presented in Table 1. As described in our previous work [9], the MCM-41 possesses the highest surface area (S_{BET}), pore volume (Vp) and pore diameter (Dp). The S_{BET}, Vp and Dp decrease slightly after the incorporation of Al, Zr and Ti, whereas the wall thickness shows the opposite trend. At the same time, from Table 1, significant decrease in the S_{BET} and Vp is observed when Ni and W species are impregnated to all the MCM-41 supports. The decrease in the S_{BET} and Vp is due to the dilution of the MCM-41 by Ni and W phases [14]. Also, the occupation and the blockage of pores by the metal particles may lead to the decrease in the S_{BET} and Vp [15]. Among all the catalysts, the NiW catalyst is found to have a minimum Dp of 3.05 nm, which may be one

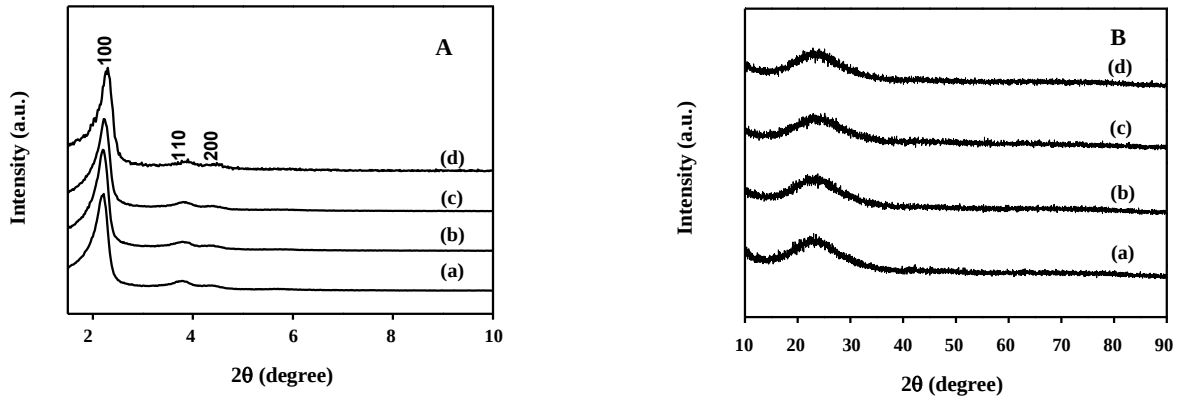

Fig. 1: Small-angle XRD patterns (A) and wide-angle XRD patterns (B) of supports: a MCM-41, b Ti-MCM-41, c Zr-MCM-41, d Al-MCM-41

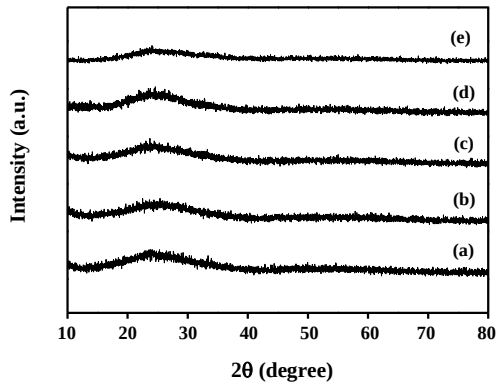

Fig. 2: XRD patterns of catalysts: a NiW, b NiW/Ti, c NiW/Zr, d NiW/Al, e Ni/W/Al

of the reason for the lowest HDN activity over NiW catalys. Moreover, the S_{BET}, Vp and Dp are similar in magnitude for the catalyst NiW/Al and Ni/W/Al.

The N_2 adsorption isotherms and pore size distribution of the supports and catalysts are shown in Fig. 3A and B. They show that the sharpness of the step (Fig. 3A) of the catalysts is much lower than that of the supports, which indicates the uniformity of mesopore size distribution according to the literature [16]. Therefore, the uniformity of mesopore size distribution decreases for the catalysts, especially the catalyst of NiW. Moreover, it can be seen from Fig. 3B, the pore size distribution changes narrowly in the catalysts relative to supports, it reflects the formation of particles inside the pores [17]. Moreover, Fig. 3 shows that the NiW/Al catalyst exhibits the similar N_2 adsorption isotherms and pore size distribution with the Ni/W/Al catalyst.

Py-IR spectra of the supports and catalysts

The surface acidity of the supports and catalysts was determined by the Py-IR technique. Usually, the bands at approximately 1450, 1595, 1606 and 1621 cm^{-1} are assigned to Lewis acid sites, while the bands at around 1540 and 1639 cm^{-1} are assigned to Brönsted acid sites. In addition, the band at 1490 cm^{-1} can be associated with pyridine adsorbed on both Lewis and Brönsted acid sites [18]. The Py-IR spectra of supports and catalysts recorded at 200 ^oC are presented in Fig. 4A and B. The bands assigned to Brönsted acid sites are not observed on the surface of MCM-41, which is consistent with our previous paper [9]. However, both the bands assigned to Lewis and Brönsted acid sites are observed on the surface of modified supports. It indicates that the incorporation of Al, Zr and Ti into MCM-41 can introduce Brönsted acid sites into the modified supports. From the Fig 4B, it can be found that both the bands assigned to Lewis and Brönsted acid sites are observed on the surface of all the catalysts.

The density of acid sites on the surface of the supports and catalysts at different temperatures is listed in Table 2. It clearly shows that density of acid sites on the surface of the supports follows the order of Al-MCM-41 > Zr-MCM-41 > Ti-MCM-41 > MCM-41. The density of acid sites on the surface of the catalysts follows the order of NiW/Al > NiW/Zr > NiW/Ti > NiW. As a result, the incorporation of Al, Zr and Ti into MCM-41 can enhance the density of acid sites on the surface of the modified supports and the corresponding catalysts, especially for the support of Al-MCM-41 and the catalyst of NiW/Al. Moreover, for comparison, the density of acid sites

Table 1: Textural properties of the supports and catalysts.

Sample	S_{BET}[a]	D_p[b]	V_p[c]	a_o[d]	W_p[e]
	($m^2 \cdot g^{-1}$)	(nm)	($cm^3\ g^{-1}$)	(nm)	(nm)
MCM-41	1071.00	3.83	1.08	4.81	0.97
Ti-MCM-41	980.30	3.23	0.89	4.81	1.58
Zr-MCM-41	969.41	3.26	0.86	4.76	1.50
Al-MCM-41	980.60	3.31	0.91	4.72	1.41
NiW	601.09	3.05	0.44	-	-
NiW/Ti	552.60	3.22	0.44	-	-
NiW/Zr	637.50	3.23	0.50	-	-
NiW/Al	597.78	3.27	0.49	-	-
Ni/W/Al	598.13	3.25	0.46	-	-

[a] *S_{BET}, specific surface area calculated by the BET method.*
[b] *D_p, pore diameter corresponding to the maximum of the pore size distribution obtained from the adsorption isotherm by the BJH method.*
[c] *V_p, pore volume determined by nitrogen adsorption at a relative pressure of 0.99.*
[d] *a_o , unit-cell parameter determined from the position of the (1 0 0) diffraction line as $a_o=2d_{(100)}/\sqrt{3}$.*
[e] *W_p, pore wall thickness of MCM-41 materials calculated by subtracting of pore diameter (D_p) from the unit-cell parameter (a_o).*

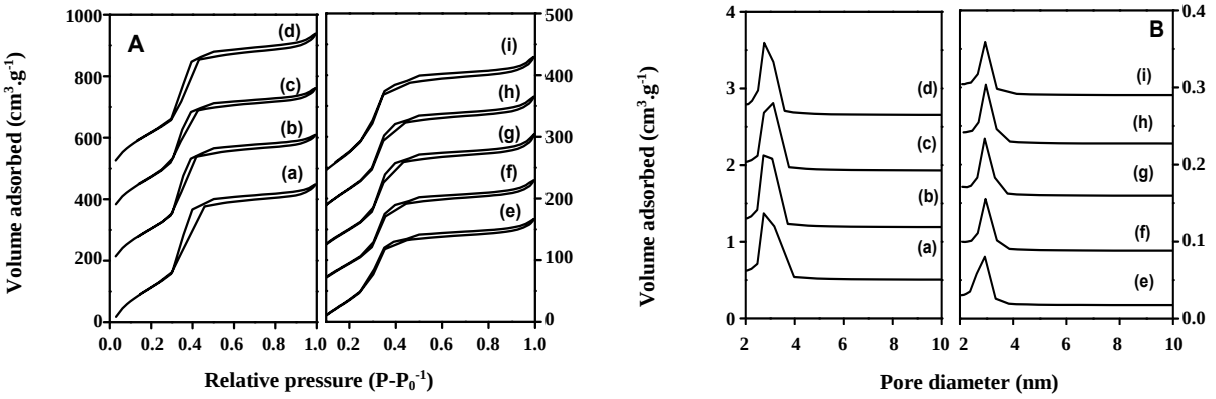

Fig. 3: N_2 adsorption-desorption isotherms (A) and Pore size distribution curves (B) of the supports and catalysts: a MCM-41, b Ti-MCM-41, c Zr-MCM-41, d Al-MCM-41, e NiW, f NiW/Ti, g NiW/Zr, h NiW/Al, i Ni/W/Al

on the surface of the Ni/W/Al catalyst also is listed in the Table 2. It can be found that the density of acid sites on the surface of the NiW/Al catalyst is higher than that of the Ni/W/Al. It indicates that the co-impregnation method can enhance the density of acid sites.

Raman spectra

To investigate the nature of metal oxide phase presented on the catalysts, Raman spectra were employed. The Raman spectra are exhibited in Fig. 5. According to the literature, the MCM-41 does not present Raman band [19]. The crystalline WO_3 presents the bands of 804, 710 and 274 cm^{-1} [19]. In addition, the band at 970 cm^{-1} is assigned to the symmetric stretching of the W=O band in octahedral polytungstate species, the band of 883 cm^{-1} is assigned to the $NiWO_4$ [20], and a shoulder at around 811 cm^{-1} reflects the Ni-W-O stretching vibrations [19, 21].

Fig. 5 shows that the band assigned to the octahedral polytungstate species (970 cm^{-1}) is observed for all the catalysts and its intensity is higher for the catalysts of NiW/M (M=Al, Zr and Ti) than that for the catalyst of NiW. Furthermore, the bands assigned to crystalline WO_3 (804 and 710 cm^{-1}) and $NiWO_4$ (883 cm^{-1}) are observed

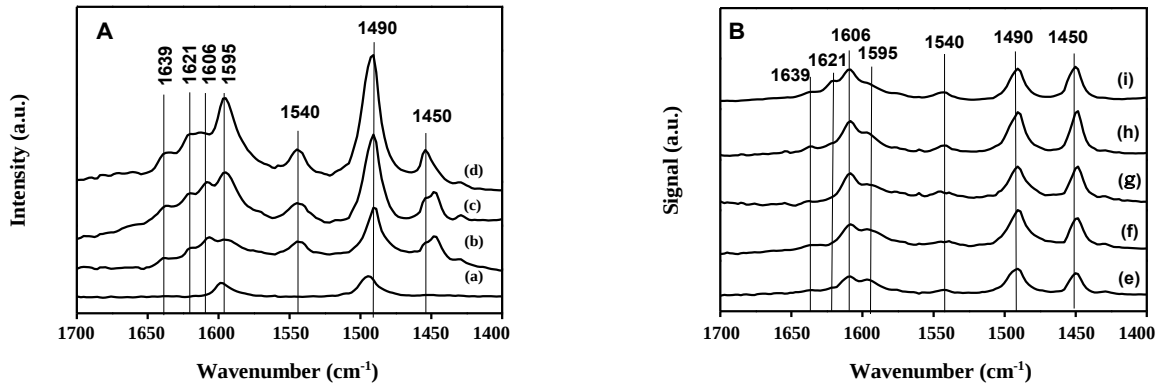

Fig. 4: Py-IR spectra of the supports (A) and catalysts (B): a MCM-41, b Ti-MCM-41, c Zr-MCM-41, d Al-MCM-41, e NiW, f NiW/Ti, g NiW/Zr, h NiW/Al , i Ni/W/Al.

for the catalyst of NiW. On the contrary, no bands assigned to them are observed for the catalysts of NiW/M (M=Al, Zr and Ti), whereas a shoulder assigned to the Ni-W-O (811 cm^{-1}) species is observed. Hence, it can be concluded that the incorporation of Al, Zr and Ti into the MCM-41 enhances the formation of octahedral polytungstate species and the Ni-W-O species. This may be due to the stronger interaction of W species with the amorphous oxides (Al_2O_3, ZrO_2 and TiO_2) than that with silica. According to the literature [22], the octahedral polytungstate species and Ni-W-O species are precursors of active species for hydrotreating catalyst. Hence, it can be concluded that the incorporation of Al, Zr and Ti into the MCM-41 favors the formation of the appropriate nature of W species on the catalysts. From the insert curve in Fig. 5, it can be found that the bands assigned to crystalline WO_3 (804 and 710 cm^{-1}) and $NiWO_4$ (883 cm^{-1}) are observed for the catalyst of Ni/W/Al. On the contrary, no bands assigned to them are observed for the catalyst of NiW/Al. Therefore, the co-impregnation favors the formation of the appropriate nature of W species.

Moreover, as mentioned above about the wide-angle XRD, no crystalline phases due to crystalline WO_3 and $NiWO_4$ are detected in the XRD patterns for the catalysts of NiW and Ni/W/Al. This discrepancy may be attributed to that the crystalline WO_3 and $NiWO_4$ crystal size is below the detection limit of the XRD technique.

XPS

The chemical state and surface composition for all the catalysts were revealed by XPS. The W4f and Ni2p spectra of the catalysts are shown in Fig. 6. It can be seen that no significant change is observed in the spectra of W4f and Ni2p for all the catalysts. The binding energies (BE) of the W4f, Ni2p are listed in Table 4. The W4f core level spectra of all the catalysts show a $W4f_{7/2}$ and $W4f_{5/2}$ doublet centered at BE about 35.8 eV and 38.0 eV, respectively. Similarly, the Ni2p core level spectra of all the catalysts show a $Ni2p_{3/2}$ and $Ni2p_{1/2}$ doublet centered at BE about 856.0 eV and 873.8 eV, with the corresponding shake-up satellite at BE about 862.3 eV and 880.5 eV. Therefore, W4f and Ni2p XPS spectra of all the catalysts have similar peak shape at similar binding energy. According to the literature, the BE of $W4f_{7/2}$ spectrum in the range of 35.8-36.5 eV ascribed to WO_3 and/or $NiWO_4$ [23], and the BE of $Ni2p_{3/2}$ spectrum in the range of 855.7-856.5 eV ascribed to Ni_2O_3 and /or $NiWO_4$ [24]

It is stated that the ratio of the metal-to-support from the XPS result can provide the important information regarding the dispersion of the metal species [24]. Thus, the ratios of W/Si and Ni/Si on the catalysts are calculated and the results are given in Table 3. It can be seen that the surface atomic ratio of W/Si follows the order of NiW/Al (0.145) > NiW/Zr (0.064) > NiW/Ti (0.059) > NiW (0.043). This tendency is also valid for the surface atomic ratio of Ni/Si and it follows the order of NiW/Al (0.062) > NiW/Zr (0.057) > NiW/Ti (0.039) > NiW (0.017). Thus, it can be concluded that the incorporation of Al, Zr and Ti into MCM-41 has a favorable effect on the dispersion of W and Ni species on the catalysts. In addition, the surface atomic ratio of W/Si

Table 2: Acidity results for the supports and catalysts.

Sample	Brönsted acidity (μmol pyridine / g)			Lewis acidity (μmol pyridine / g)		
	100 °C	200 °C	250 °C	100 °C	200 °C	250 °C
MCM-41	17.5	0	0	99.5	0	0
Ti-MCM-41	43.9	34.0	26.3	174.6	42.3	19.6
Zr-MCM-41	92.3	61.8	44.4	235.5	62.3	37.2
Al-MCM-41	118.3	80.5	51.7	371.7	150.3	58.6
NiW	33.9	10.0	5.1	170.5	57.4	39.8
NiW/Ti	47.8	22.1	5.9	220.5	84.7	55.3
NiW/Zr	51.3	26.5	6.4	243.6	93.1	64.7
NiW/Al	70.8	39.8	23.9	282.4	186.7	84.5
Ni/W/Al	61.4	35.1	20.8	199.4	112.1	75.5

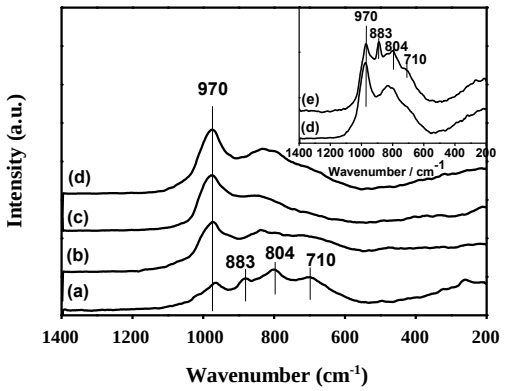

Fig. 5: Raman spectra of catalysts: a NiW, b NiW/Ti, c NiW/Zr, d NiW/Al , e Ni/W/Al.

and Ni/Si on the catalyst of Ni/W/Al also are listed in the Table 4. It can be found that the surface atomic ratio of W/Si on the NiW/Al catalyst is higher than that of Ni/W/Al. Therefore, the co-impregnation method can enhance the dispersion of W species. However, the tendency of Ni/Si is contrary to that of W/Si. It can be interpreted by that the Ni species for the Ni/W/Al catalyst is impregnated after W species, leading to the enrichment of Ni species on the surface of Ni/W/Al catalyst.

H_2-TPR

The reducibility of the catalysts was characterized by H_2-TPR experiment. Reduction profiles of the catalysts are presented in Fig. 7. The TPR profiles of all catalysts show two principal reduction peaks in the temperature ranges of 500-700 °C and >800 °C, respectively. The low temperature peak (500-700 °C) can be ascribed to the reduction of polymeric octahedral tungsten species and the broad peak at high temperature (>800 °C) can be assigned to the superimposed reduction of tetrahedrally coordinated tungsten species [25, 26]. Moreover, the maximum reduction temperature of the catalysts in the temperature range of 500-700 °C follows the order of NiW (613 °C) > NiW/Ti (566 °C) > NiW/Zr (553 °C) > NiW/Al (543 °C), indicating that the incorporation of Al, Zr and Ti into MCM-41 leads to an easier reduction of polymeric octahedral tungsten species on the catalysts. The reason for this is better dispersion of W species on the catalysts with Al, Zr and Ti [27, 28]. The decrease of reduction temperature favors for the reduction and sulphidation of the W species leading to the formation of more active species [29]. Moreover, compared with the catalyst NiW/Al, catayst Ni/W/Al exhibits the same magnitude of maximum reduction temperature and the decrease in H_2 consumption in the temperature range of 500-700 °C. The same magnitude of maximum reduction temperature may be attributed that the interaction between the metal species and Al-MCM-41 is almost equal for catayst NiW/Al and Ni/W/Al. The decrease in H_2 consumption for catayst Ni/W/Al may be attributed to the decrease in the relative amount of polymeric octahedral tungsten species for the NiW/Al catayst.

SEM

In order to investigate the morphology of the catalysts, the SEM characterization was carried out and shown in Fig. 8. It shows that the incorporation of Al, Zr

Table 3: The binding energies of the W4f, Ni2p and the ratios of W/Si, Ni/Si.

Catalyst	Binding energy (eV)				W/Si	Ni/Si
	$W4f_{7/2}$	$W4f_{5/2}$	$Ni2p_{3/2}$	$Ni2p_{1/2}$		
NiW	35.8	37.9	855.7	873.9	0.043	0.017
			862.3	880.6		
NiW/Ti	35.7	37.9	856.0	873.8	0.059	0.039
			862.2	880.5		
NiW/Zr	35.7	37.9	856.1	873.8	0.064	0.057
			862.3	880.6		
NiW/Al	35.8	37.9	855.9	873.8	0.145	0.062
			862.3	880.3		
Ni/W/Al	35.8	37.9	856.2	873.8	0.140	0.217
			862.3	880.6		

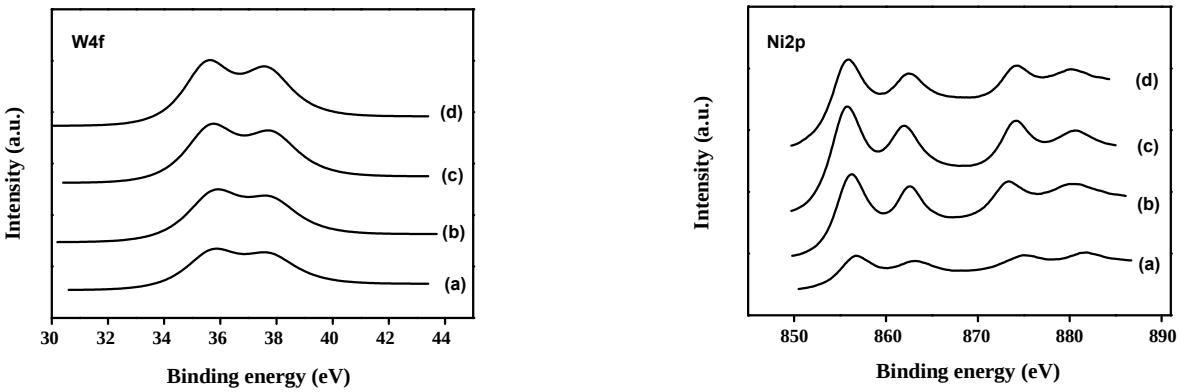

Fig. 6: W4f and Ni2p spectra of the catalysts: a NiW, b NiW/Ti, c NiW/Zr, d NiW/Al.

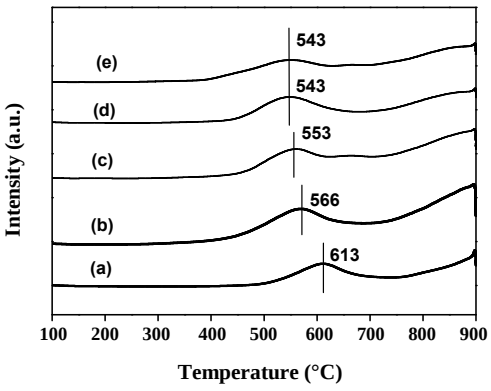

Fig. 7: The H_2-TPR spectra of the catalysts: a NiW, b NiW/Ti, c NiW/Zr, d NiW/Al, e Ni/W/Al.

and Ti remarkably affects the morphology of the catalysts. The catalysts of NiW and NiW/Ti display some large particles with irregular shape due to the aggregation between smaller particles, especially for the catalyst of NiW. However, the catalysts of NiW/Zr and NiW/Al only display small particles with irregular shape. Besides, the small particles in the catalyst of NiW/Al are best dispersed among all the catalysts. It can be concluded that the incorporation of Al, Zr and Ti can enhance the dispersion of particles on the catalyst, especially the catalyst of NiW/Al.

Hydrodenitrogenation

The effects of reaction temperature on the conversion and HDN activity of quinoline over catalysts are

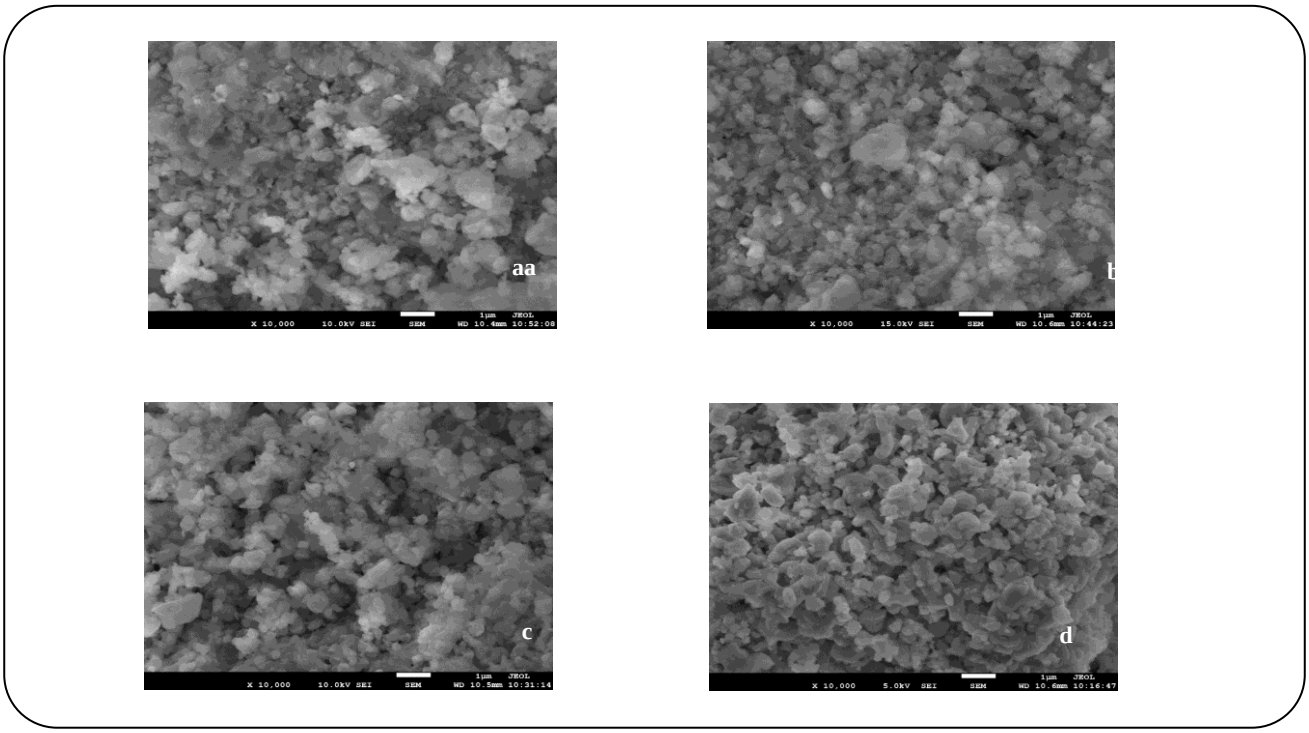

Fig. 8: SEM micrographs of catalysts: a NiW, b NiW/Ti, c NiW/Zr, d NiW/Al.

compared in Fig. 9. It clearly shows that the conversion of quinoline is above 95% in the range of reaction temperatures investigated for all the catalysts. It indicates that quinoline can be hydrogenated easily to hydrogenation products. Fig. 9 also shows that the HDN activity increases with the increasing reaction temperature for all the catalysts. Moreover, it can be found that the HDN activity follows the order of NiW/Al > NiW/Zr > NiW/Ti > NiW. It indicates that the incorporation of Al, Zr and Ti is favorable for the HDN of quinoline, which is well agreement with the result of our previous work [9]. In the present work, the catalyst of NiW/Al exhibits the highest catalytic activity with HDN of 39 % at 350 ^{o}C and 90 % at 390 ^{o}C, whereas the catalyst of NiW exhibits the lowest catalytic activity with HDN of 17 % at 350 ^{o}C and 54 % at 390 ^{o}C. The highest catalytic activity on NiW/Al can be attributed to the well dispersion of W and Ni species, the higher density of acid sites, the more appropriate nature of W species and the lower reduction temperature of W species on the catalyst of NiW/Al than that on the other catalysts. To make a quantitative analysis, the ratio of HDN activity at 370 ^{o}C, density of acid sites (Py-IR, at 200 ^{o}C) , W/Si and Ni/Si (XPS) of the different catalysts are presented in Table 4. The ratio of HDN (NiW/M (M=Al, Zr or Ti))/ HDN (NiW) of the different catalysts follows the order of NiW/Al (2.30) > NiW/Zr (1.68) > NiW/Ti (1.22). This tendency is also valid for the density of acid sites, W/Si and Ni/Si of the different catalysts. It indicates that there is positive correlation between the HDN activity and the density of acid sites, the dispersion of W and Ni species of the catalysts.

Moreover, compared with our previous work about the catalysts prepared by sequential impregnation method using modified MCM-41 as supports [9], the HDN results showed that the catalysts prepared by co-impregnation method are more active than the catalysts prepared by sequential impregnation method. It should be noted that, no matter what kind of impregnation method, the optimum HDN activity was observed on the catalyst supported on the Al modified MCM-41. In this paper, the Ni/W/Al catalyst is chosen as an example due to its high HDN activity, which exhibits the catalytic activity with HDN of 37 % at 350 ^{o}C and 85 % at 390 ^{o}C. As discussed above, compared with the Ni/W/Al catalyst, the NiW/Al catalyst possesses the higher density of acid sites (Py-IR), the more

Table 4: The ratios of HDN, density of acid sites, W/Si and Ni/Si (NiW/M (M=Al, Zr or Ti)/(NiW)).

Catalyst	HDN	(Brönsted + Lewis) acidity	W/Si	Ni/Si
NiW	1	1	1	1
NiW/Ti	1.22	1.58	1.37	2.29
NiW/Zr	1.68	1.77	1.48	3.35
NiW/Al	2.30	3.36	3.37	3.65
Ni/W/Al	2.01	2.18	3.25	12.76

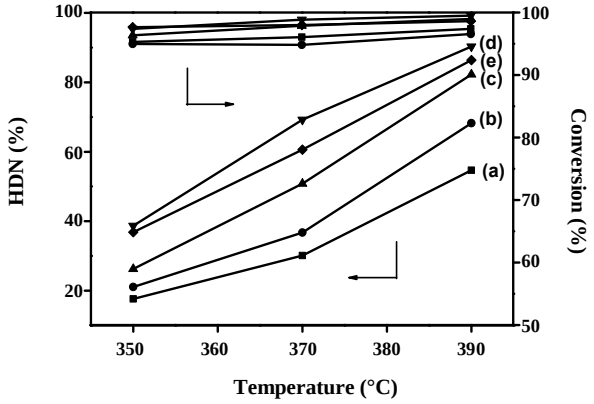

Fig. 9: Conversion and HDN of quinoline as a function of temperature for catalysts: a NiW, b NiW/Ti, c NiW/Zr, d NiW/Al, e Ni/W/Al.

dispersion of W species (XPS) and the more appropriate nature of W species (Raman).

An important observation is that the HDN activity over the Ni/W/Al catalyst is higher than that over the NiW/Zr and NiW/Ti catalysts for all investigated temperatures. This result is not consistent with the result of the Raman. As mentioned above, the Raman shows that compared with the NiW/Zr and NiW/Ti catalysts, the Ni/W/Al catalyst contains some unfavourable nature of W species (crystalline WO_3 and $NiWO_4$). However, the Py-IR and XPS show the opposite result. Compared with the NiW/Zr and NiW/Ti catalysts, the Ni/W/Al catalyst shows higher density of acid sites (Py-IR) and more dispersion of W species (XPS). An explanation for this phenomenon may be that the density of acid sites and dispersion of W species are important than the nature of W species for HDN activity of catalyst.

The HDN reaction network of quinoline is shown in Fig. 10. Generally, the N in the quinoline can be removed via the saturated intermediates pathway (Q→DHQ→PCHA→PCH+PCHE) and the aromatic intermediates pathway (Q→THQ1→OPA→PB) (Fig. 10).

The product distribution for HDN of quinoline over the catalyst of NiW/Al is presented in Fig. 11. The main products are THQ1, THQ5, DHQ, PCH and PB. With increasing of the temperature, the C-N band cleavage is significantly accelerated, leading to the decreased selectivity of THQ1, THQ5 and DHQ, and the increased selectivity of the final products of PB and PCH.

For different catalysts, the selectivity of PCH and PB at all investigated temperature follows the order of NiW/Al > NiW/Zr > NiW/Ti > NiW (Fig. 12). This reveals that the incorporation of Al, Zr and Ti into MCM-41 enhances both the fully hydrogenated intermediates pathway and the partially hydrogenated intermediates pathway.

CONCLUSIONS

The Al, Zr and Ti modified MCM-41 were prepared by postsynthetic method and were used as supports for NiW catalysts, which were prepared by co-impregnation method and used in HDN of quinoline. The characterization of the catalysts revealed that the incorporation of Al, Zr and Ti into MCM-41 promoted the dispersion of W and Ni species, the density of acid sites, the formation of appropriate nature of W species and the decrease the reduction temperature of W species on the catalysts, especially Al. The HDN results showed that the catalyst of NiW/Al exhibited the highest HDN activity among all the catalysts. Moreover, the catalyst

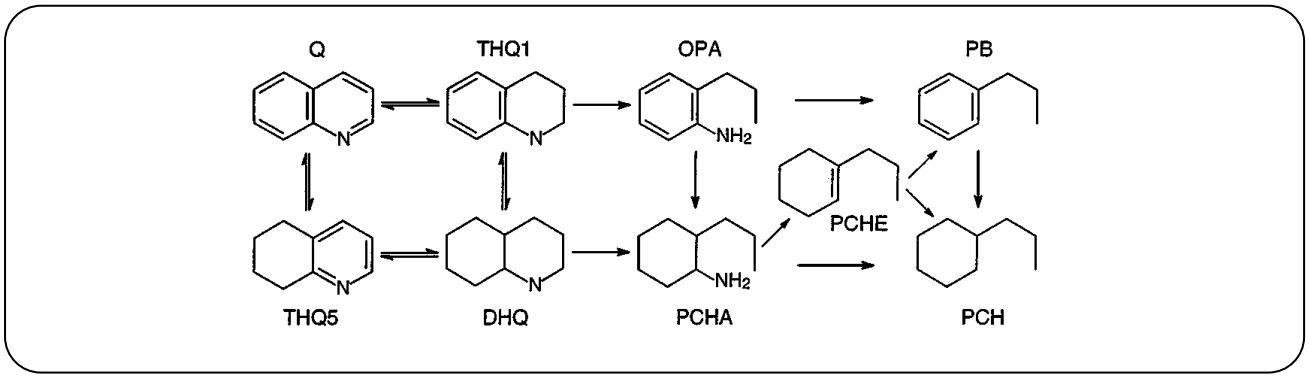

Fig. 10: HDN reaction network of quinolone. Q quinoline, THQ5 5,6,7,8-tetrahydroquinoline, DHQ decahydroquinoline, THQ1 1,2,3,4-tetrahydroquinoline, OPA ortho-propylaniline, PCHA 2-propylcyclo-hexylamine, PCHE propylcyclohexene, PCH propylcyclohexane, PB propylbenzene.

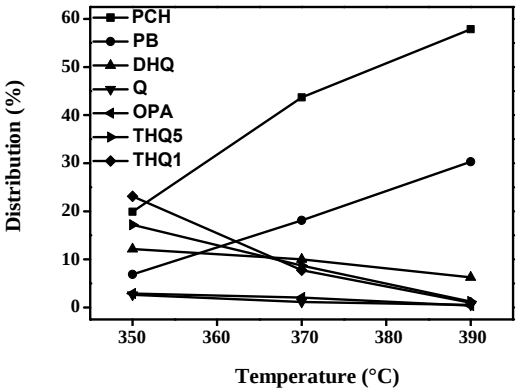

Fig. 11: Product distribution for HDN of quinoline on the catalyst of NiW/Al.

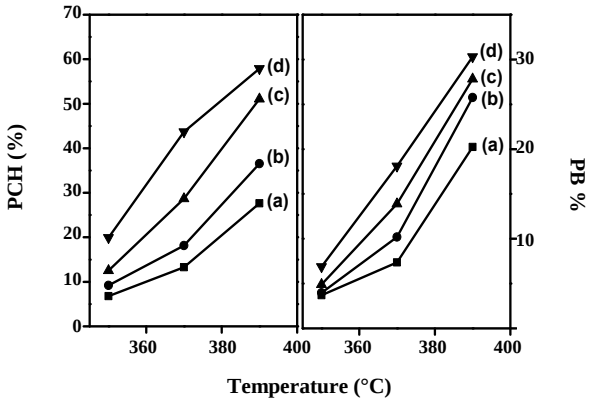

Fig. 12: Selectivity of PCH and PB as a function of temperature for catalysts: a NiW, b NiW/Ti, c NiW/Zr, d NiW/Al.

of NiW/Al showed better HDN performance than the catalyst of Ni/W/Al.

Received : Aug. 4, 2018 ; Accepted : Nov. 23, 2018

REFERENCES

[1] Kanda Y., Temma C., Nakata, K., Kobayashi T., Sugioka M., Uemichi Y., Preparation and Performance of Noble Metal Phosphides Supported on Silica as New Hydrodesulfurization Catalysts, *Appl. Catal. A: Gen.*, **386**: 171-178 (2010).

[2] Yu G.L., Zhou Y.S., Wei Q., Tao X.J., Cui Q.Y., A Novel Method For Preparing Well Dispersed and Highly Sulfided Niw Hydrodenitrogenation Catalyst, *Catal. Commun.*, **23**: 48-53 (2012).

[3] Klimova T., Gutiérrez O., Lizama L., Amezcua J., Advantages of ZrO_2- and TiO_2–SBA-15 Mesostructured Supports for Hydrodesulfurization Catalysts over Pure TiO_2, ZrO_2 and SBA-15, *Micropor. Mater.*, **133**: 91-99 (2010).

[4] Gutiérrez O.Y., Ayala E., Puente I., Klimova T., Application of New ZrO_2-SBA-15 Materials as Catalytic Supports: Study of Intrinsic Activity of Mo Catalysts in Deep HDS, *Chem. Eng. Comm.*, **196**: 1163-1177 (2009).

[5] Herrera J.M., Reyes J., Roquero P., Klimova T., New hydrotreating NiMo Catalysts Supported on MCM-41 Modified with Phosphorus, *Micropor. Mater.*, **83**: 283-291 (2005).

[6] Silva-Rodrigo R., Calderón-Salas C., Melo-Banda J.A., Domínguez J.M., Vázquez-Rodríguez A. Synthesis, Characterization and Comparison of Catalytic Properties of NiMo- and NiW/Ti-MCM-41 catalysts for HDS of Thiophene and HVGO, *Catal. Today*, **98**: 123-129 (2004).

[7] Klimova T., Calderón M., Ramírez J., Ni and Mo Interaction with Al-Containing MCM-41 Support and Its Effect on the Catalytic Behavior in DBT Hydrodesulfurization, *Appl. Catal. A: Gen.*, **240**: 29-40 (2003).

[8] Rodríguez-Castellõn E., Jimenez-Lõpez A., Eliche-Quesada D., Nickel and Cobalt Promoted Tungsten and Molybdenum Sulfide Mesoporous Catalysts tor Hydrodesulfurization, *Fuel*, **87**: 1195-1206 (2008).

[9] Guo F., Guo S., Wei X.X., Wang X., Xiang H., Qiu Z., Zhao L., MCM-41 Supports Modified by Al, Zr and Ti for NiW Hydrodenitrogenation Catalysts, *Catal. Lett.*, **144**: 1584-1593 (2014).

[10] Salerno P., Mendioroz S., López Agudo A., Al-Pillared Montmorillonite-Based Nimo Catalysts for HDS and HDN of Gas Oil: Influence of the Method and Order of Mo And Ni Impregnation, *Appl. Catal. A: Gen.*, **259**: 17-28 (2004).

[11] Sardhar Basha S.J., Vijayan P., Suresh C., Santhanaraj D., Shanthi K., Effect of Order of Impregnation of Mo and Ni on the Hydrodenitrogenation Activity of Nio-Moo_3/Almcm-41 Catalyst, *Ind. Eng. Chem. Res.*, **48**: 2774-2780 (2009).

[12] Khder A.E.R.S., Hassan H.M.A., El-Shall M.S. Acid Catalyzed Organic Transformations by Heteropoly Tungstophosphoric Acid Supported on MCM-41, *Appl. Catal. A: Gen.*, **411-412**: 77-86 (2012).

[13] Carriazo D., Domingo C., Martín C., Rives V., Pmo or PW Heteropoly Acids Supported on MCM-41 Silica Nanoparticles: Characterisation and FT-IR Study of the Adsorption of 2-Butanol, *J. Solid State Chem.*, **181**: 2046-2057 (2008).

[14] Méndez F.J., Llanos A., Echeverría M., Jáuregui R., Villasana Y., Díza Y., Liendo-Polanco G., Ramos-García M.A., Zoltan T., Brito J.L., Mesoporous Catalysts Based on Keggin-Type Heteropolyacids Supported on MCM-41 and Their Application in Thiophene Hydrodesulfurization, *Fuel*, **110**: 249-258 (2013).

[15] Palcheva R., Spojakina A., Dimitrov L., Jiratova K., 12-Tungstophosphoric Heteropolyacid Supported on Modified SBA-15 as Catalyst in HDS of Thiophene, *Micropor. Mater.*, **122**: 128-134 (2009).

[16] Luo Y., Hou Z., Li R., Zheng X., Rapid Synthesis of Ordered Mesoporous Silica with the Aid of Heteropoly Acids, *Micropor. Mater.*, **109**: 585-590 (2008).

[17] Vradman L., Landau M.V., Kantorovich D., Koltypin Y., Gedanken A., Evaluation of Metal Oxide Phase Assembling Mode Inside the Nanotubular Pores of Mesostructured Silica, *Micropor. Mater.*, **79**: 307-318 (2009).

[18] Kalita P., Gupta N.M., Kumar R., Synergistic Role of Acid Sites In The Ce-Enhanced Activity of Mesoporous Ce–Al-MCM-41 Catalysts in Alkylation Reactions: FTIR and TPD-Ammonia Studies, *J. Catal.*, **245**: 338-347 (2007).

[19] Chen H., Dai W.L., Deng J.F., Fan K., Novel Heterogeneous W-Doped MCM-41 Catalyst for Highly Selective Oxidation of Cyclopentene to Glutaraldehyde by Aqueous H_2O_2, *Catal. Lett.*, **81**: 131-136 (2002).

[20] Xiao T., Wang H., York A.P.E., Williams V.C., Green M.L.H., Preparation of Nickel–Tungsten Bimetallic Carbide Catalysts, *J. Catal.*, **209**: 318-330 (2002).

[21] Tayeb K.B., Lamonier C., Lancelot C., Fournier M., Payen E., Bonduelle A., Bertoncini F., Study Of The Active Phase of Niw Hydrocracking Sulfided Catalysts Obtained from an Innovative Heteropolyanion Based Preparation, *Catal. Today*, **150**: 207-212 (2010).

[22] Lei Z., Gao L., Shui H., Chen W., Wang Z., Ren S., Hydrotreatment of Heavy Oil from a Direct Coal Liquefaction Process on Sulfided Ni–W/SBA-15 Catalysts, *Fuel Process. Technol.*, **92**: 2055-2060 (2011).

[23] Ding L., Zheng Y., Zhang Z., Ring Z., Chen J., Hydrotreating of Light Cycle Oil Using Wni Catalysts Containing Hydrothermally and Chemically Treated Zeolite Y, *Catal. Today*, **125**: 229-238 (2007).

[24] Salvatl L., Makovsky L.E., Stencel J.M., Brown F.R., Hercules D.M., Surface Spectroscopic Study of Tungsten-Alumina Catalysts Using X-Ray Photoelectron, Ion Scattering, and Raman Spectroscopies, *J. Phys. Chem.*, **85**: 3700-3707 (1981).

[25] Wan G., Duan A., Zhang Y., Zhao Z., Jiang G., Zhang D., Liu J., Chung K., Niw/AMBT Catalysts for the Production of Ultra-Low Sulfur Diesel, *Catal. Today*, **158**: 521-529 (2010).

[26] Lizama L.Y., Klimova T.E., SBA-15 Modified with Al, Ti, or Zr as Supports for Highly Active Niw Catalysts for HDS, *J. Mater. Sci.*, **44**: 6617-6628 (2009).

[27] Fan Y., Bao X., Wang H., Chen C., Shi G., A Surfactant-Assisted Hydrothermal Deposition Method for Preparing Highly Dispersed W/Γ-Al_2O_3 Hydrodenitrogenation Catalyst, *J. Catal.*, **245**: 477-481 (2007).

[28] Saadatjou N., Jafari A., Sahebdelfar S., Synthesis and Characterization of Ru/Al_2O_3 Nanocatalyst for Ammonia Synthesis, *Iran. J. Chem. Chem. Eng. (IJCCE)*, **34**(1): 1-9 (2015).

[29] Wei Q., Zhou Y., Wen S., Xu C., Preparation and Properties of Nickel Preimpregnated CYCTS Supports for Hydrotreating Coker Gas Oil, *Catal. Today*, **149**: 76-81 (2010).